VIBRATION FIELD OF A DOUBLE-LEAF PLATE WITH RANDOM PARAMETER FUNCTIONS

Hyuck Chung

School of Computing and Mathematical Sciences, Auckland University of Technology, PB 92006, Auckland, New Zealand

hchung@aut.ac.nz

This paper shows how to compute vibrations of a double-leaf plate with random inhomogeneities in its components. The components are two plates and reinforcement beams. The modelling method is based on the variational principle for elastic plates and beams. In addition to the deformation of individual components, the model includes contributions from junctions between components, e.g., rigidly of the connection between a beam and a plate. The model does not restrict the junctions to be perfectly straight. The beams are allowed to have a small random twist. The junction rigidity is included as potential energy in addition to the strain and the kinetic energies of the components. The random inhomogeneities are simulated as continuous smooth random functions. A random function is realized using a predetermined probability density function and a power spectral density function. The vibration is then computed from a set of random functions. The numerical simulations show that the random stiffness affects the behaviour of the structure in a wide frequency range. Whereas the junctions affect the a lower frequency vibrations. The root-mean-square velocity of surface vibration level shows changes at resonance frequencies depending on the random functions.

INTRODUCTION

This paper presents a theoretical and computational model of vibrations of a double-leaf plate when it is subjected to some external forces. Double-leaf plates have a high strength-to-weight ratio, and are used in many lightweight constructions. Acoustic properties of double-leaf plates are more difficult to predict than those of single plates, because of a high number of components that make up typical double-leaf plates. A simple design of a double-leaf plate would have two plates sandwiching reinforcement parallel beams. There are various methods of joining the two components such as nails and glue. The large number of distinct components and the complexity of the junctions make the mathematical representation of the double-leaf plate difficult. The often used finite element method (FEM) would represent the junction between a plate and a beam as a 'T' shaped continuous object. This is not true in most cases because the connection at the junction is not perfect, while additionally the material properties of the plate and the beam may be completely different. In other cases, the FEM would require microscopic descriptions of the junction, for example describing how the nails react to various forces and affect the surrounding material. This paper uses an alternative way of modelling the junctions. A junction is modelled by the amount of energy required for any particular way of deformation of the junction. The amount of energy at the junction will be large or small if the bonding is strong or weak.

The conventional deterministic models of double-leaf plates that use the partial differential equations of Kirchhoff plates and Euler beams can predict low frequency vibrations (see [1, 2, 7, 8, 9]). The parameters of the equations are constants such as mass density and Young's modulus. However the vibration of a double-leaf plate becomes unpredictable above the 5th resonant frequency, which in the case of a 3.2m-by-5.1m structure is about 80 Hz. This particular dimension is chosen because of author's past experience with an experimental programme on timber-framed floor/ceiling systems (see [2]). One can find variations in the vibrations of apparently identical composite structures. The discrepancy may come from the manufacturing inconsistencies or random inhomogeneities in the components themselves. The unpredictability of the vibrations of composite structures have been known for many years, and modelled using various methods such as perturbation, scattering, and asymptotic methods. All of these methods assume the irregularities in the structure to be small compared to the wavelengths, and hence terms higher than first-order are negligible. This is not true for most engineered products.

Another popular modelling method for double-leaf plates is Statistical Energy Analysis (SEA). In order to use SEA, a structure needs to be divided into sub-systems that interact with their neighbouring systems. Two neighbouring sub-systems are related by a loss factor that is determined either from experiments or theoretical models. Measurements and theoretical predictions of various types of double-leaf plates are considered in [3, 4]. SEA has been used successfully to predict the surface vibration level above 300 Hz. However SEA is not suitable for computing the vibrations in the frequency range of concern here.

In this paper the deformation of each component is computed using the variational principle. The energy density functions for individual components and junctions are derived using the Kirchhoff plate, Euler beam models and Hooke's law. Once the integral form of the total energy in the double-leaf plate is obtained from the functions of the deformation of individual components of the double-leaf plate, the true solution will give the minimum of the integral form. The solution will be computed using the Fourier series expansion of the solution

over the basis functions in the x and y-directions, which is possible because of the rectangular shape of the structure. The irregularities, the stiffness (Young's modulus) of the two plates, junctions and the small twist in the beams, are included using their Fourier components. The Fourier representation of the solution keeps the computation cost low. The computation cost is determined by the number of Fourier terms. In this paper 20×20 terms are used for a plate and 20 terms for a beam. On the other hand, the computation cost of using FEM is dependent on the resolution of the finite element mesh that must be generated for a whole 3-dimensional double-leaf plate. The junctions will need high resolution mesh to capture the small deformation.

In addition to the simplified junction model, a few selected parameters are simulated as random functions (or random process) with pre-assigned power spectral density (PSD) functions and probability density functions (PDFs). The parameters are the stiffness of the plates, the rigidity of the junction, and shape of the beams. Each random function is assumed to be stationary, and thus its PDF is identical everywhere at any spatial location. This paper follows the method given in [6], in which only 1-dimensional examples are given. In this paper, 2-dimensional random functions are used to simulate the irregular stiffness of the top and bottom plates. The extension from 1 to 2 dimensional random function is straightforward. The computation is carried out for each of the random functions and the results (vibrations of the top plate) are studied using the root-mean-square velocity and the spatial distribution of the variance of the vibration amplitude. The computation time of, say 5000 simulations, for each random function was approximately 2 to 3 hours using MatLab on a desktop computer.

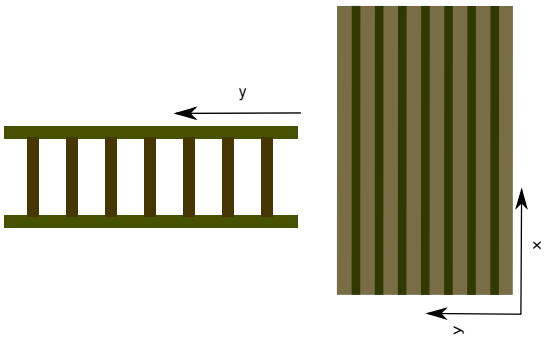

Figure 1. Depiction of a double-leaf plate. Cross section (left) and the view from the top (right). The origin of the coordinate system is at the lower corner

MODELLING AND MATHEMATICAL FORMULATION

Variational formulation

The deflection of the individual components is the solution, which will be computed in this paper. A local coordinate system is used for each component, that is, the origin is placed at the corner of each plate, and each beam has the origin at one end (see Fig. 1). Here the simple harmonic vibration is considered, and hence the solutions will have the form $\mathbf{Re}\left[w(x,y)\exp \mathrm{i}\,\omega t\right]$ where ω is the radial frequency. The deflection of each component is denoted by $w_1(x,y)$, $w_2(x,j)$, and $w_3(x,y)$ for the top plate, jth beam, and the bottom plate, respectively. Other parameters and functions will be denoted with the corresponding subscripts 1, 2, or 3 for the top plate, beams, and bottom plate, respectively. For example, the thickness of the top plate is denoted by h_1, and the mass density of the bottom plate will be ρ_3, and so on. The length (x-direction) and the width (y-direction) are A and B, respectively. Hence the plates cover the area $(x,y) \in [0,A] \times [0,B]$, and the beams are modelled as one dimensional objects for $x \in [0,A]$. The beams have the same size, density, and elastic modulus.

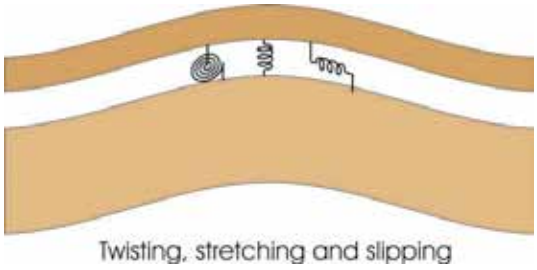

Figure 2. Depiction of the model for the coupling conditions between the plate (top) and the beam (bottom). The springs give the resistance to the rotational (left), vertical (centre), and horizontal (right) movements

We choose the variational formulation using the Lagrangian of the deflection to compute the vibration field of the structure. The vibration field of the structure is found by constructing the Lagrangian of the total energy in the structure (see [10]). The solution will be found by minimizing the Lagrangian. The Lagrangian for the whole structure is given by the following general form for the given deformation of the structure.

$$\mathscr{L} = \int_0^T \int_V \left\{ \mathscr{P}(t) + \mathscr{K}(t) - \mathscr{F}(t) \right\} dv dt, \tag{1}$$

where $\mathscr{P}$ is the potential energy, $\mathscr{K}$ is the kinetic energy, and $\mathscr{F}$ is the work done to the object. The integral is taken over the volume of the elastic body and the period of time T. Here the integral will be taken over the plates and beams. The integral over time need not be considered because the vibration is simple harmonic.

The classical Kirchhoff (thin elastic) plate model expresses the strain energy and kinetic energy of a thin elastic plate, which has non-moving boundary, by

$$\mathscr{P}_1 = \frac{1}{2} \int_0^A \int_0^B D_1(x,y) \left| \nabla^2 w_1 \right|^2 dxdy \tag{2}$$

$$\mathscr{K}_1 = \frac{\rho_1 h_1 \omega^2}{2} \int_0^A \int_0^B |w_1(x,y)|^2 dxdy \tag{3}$$

where $D_1(x,y) = E_1(x,y)h_1^3/\left(12\left(1-\alpha^2\right)\right)$ is the flexural rigidity and ρ_1, h_1, E_1 and α are the density, the plate thickness,

Young's modulus and Poisson ratio, respectively. Note that the effect of rotation is neglected in $\mathscr{K}_1$. The minima of Eq. (1) is the solution of the thin plate equation,

$$\nabla^2\left(D_1(x,y)\nabla^2 w_1(x,y)\right) - \omega^2 m_1 w_1(x,y) = p(x,y) \tag{4}$$

where $m_1 = \rho_1 h_1$ is the mass density per unit area, and p is the effective pressure acting on the plate. The above differential equation is useful when an analytical solution can be considered. We however deal with irregular structural properties, and therefore the solution method is numerical. The energies for the bottom plate are given by the same formulae with $\mathscr{P}_3$ and $\mathscr{K}_3$ for w_3.

The strain and kinetic energies for the Euler beams are given by

$$\mathscr{P}_2 = \frac{1}{2}\sum_{j=1}^{S}\int_0^A E_2 I \left|w_2''(x,j)\right|^2 dx \tag{5}$$

$$\mathscr{K}_2 = \frac{\rho_2 h_2 \omega^2}{2}\sum_{j=1}^{S}\int_0^A |w_2(x,j)|^2 dx \tag{6}$$

where E_2 and I are the Young's modulus and the moment of inertia of the beam, and $\rho_2$and h_2 are the mass density per unit length and the thickness of the beam, respectively. The primes $''$ on w indicate the second derivative with respect to x.

The combination of Kirchhoff plates and Euler beams has been used successfully in [2] to predict vibrations of timber-framed floor/ceiling systems. An example of comparison between the theoretical prediction and the experimental measurement is shown Fig. 3. Figure 3 shows the root-mean-square velocity of the bottom plate. The theoretical prediction disagrees with the experimental measurement above 80 Hz. The model of the double-leaf plate in [2] includes cavity air, damping in timber components, and various attachments used in construction of real building structures. In this paper the model is simplified to to keep the computation minimum. Furthermore the purposes of this paper are to study the effects of the randomness in the structure and show how the random functions can be included in the method of solution.

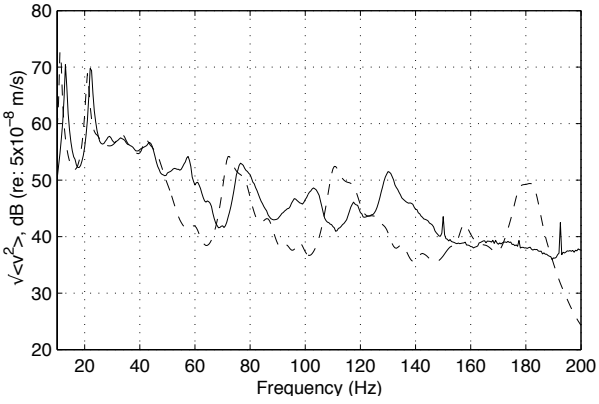

Figure 3. Comparison between the theoretical prediction (dashed) and the experimental measurements (solid)

Coupling at the junctions

In addition to the strain and kinetic energy, we include the energy contributions from the junctions due to the discrepancy in the displacement of the two components (see Fig. 2). The potential energies at the junctions are given by

$$\mathscr{P}_{1,2}^{\text{sep}} = \frac{1}{2}\sum_{j=1}^{S}\int_0^A \sigma_{\text{sep}}(x,j)\left|w_1(x,y_j) - w_2(x,j)\right|^2 dx \tag{7}$$

$$\mathscr{P}_{1,2}^{\text{slip}} = \frac{1}{2}\sum_{j=1}^{S}\int_0^A \sigma_{\text{slip}}(x,j)\left|h_1 w_1'(x,y_j) + h_2 w_2'(x,j)\right|^2 dx \tag{8}$$

$$\mathscr{P}_{1,2}^{\text{rot}} = \frac{1}{2}\sum_{j=1}^{S}\int_0^A \sigma_{\text{rot}}(x,j)\left|w_1'(x,y_j) - w_2'(x,j)\right|^2 dx \tag{9}$$

where $'$ indicates the derivative with respect to x and σ_{sep}, σ_{slip}, and σ_{rot} are the Hooke's constants for springs resisting the relative separation, slippage and rotation, respectively. These functions are defined along the beams and have the single variable x. The subscripts of $\mathscr{P}$ indicate the interaction between either top plate and beams $((1,2))$, or bottom plate and the beams $((3,2))$. A simpler model of the junction may let the separation constant σ_{sep} become very large, that is, the separation is nearly zero and the plate and the beams are always in contact. The total potential energy, $\mathscr{P}$ in Eq. (1), is the sum of all potential energies from the individual components and the junctions. In [2] the slippage at the junctions have been proven to be necessary for predicting the vibration level over the frequency range shown in Fig. 3.

Method of solution

The method of solution chosen in this paper is the Fourier expansion method, which is ideal because of the rectangular shape of the structure. Furthermore the boundary of the plate is assumed to be simply supported. Thus the basis functions are sine-functions, further simplifying the solution. Different basis functions must be chosen when the boundary conditions are different. There are a few example sets of basis functions shown in [10] for free or clamped boundaries. Whatever the basis functions may be, a linear system of equations for the coefficients of the expansion over the chosen basis functions can be formulated. Hence the method of solution shown here will be applicable.

The deflection of the top plate, bottom plate and beams are expressed by

$$w_1(x,y) = \sum_{m,n=1}^{N} C_{mn}^{(1)}\phi_m(x)\psi_n(y) \tag{10}$$

$$w_3(x,y) = \sum_{m,n=1}^{N} C_{mn}^{(3)}\phi_m(x)\psi_n(y) \tag{11}$$

$$w_2(x,j) = \sum_{m=1}^{N} C_{mj}^{(2)}\phi_m(x) \tag{12}$$

for $j = 1,2,...,S$, respectively. The basis functions are given by $\phi_m(x) = \sqrt{2/A}\sin k_m x$, and $\psi_n(y) = \sqrt{2/B}\sin\kappa_n y$, and the

wavenumbers are given by $k_m = \pi m/A$ and $\kappa_n = \pi n/B$. Note that the basis functions are orthonormal. The positions of the joists are given by $y = y_j$, $j = 1,2,...,S$. Note that the number of terms in the series has already been truncated to N to construct the finite system for the numerical computation. The operations in Eq. (1) are then expressed using the column vectors of the coefficients, $\mathbf{c_1} = \left(C_{11}^{(1)}, C_{21}^{(1)}, \cdots, C_{NN}^{(1)}\right)$, $\mathbf{c_2} = \left(C_{11}^{(2)}, C_{21}^{(2)}, \cdots, C_{NS}^{(2)}\right)$, and $\mathbf{c_3} = \left(C_{11}^{(3)}, C_{21}^{(3)}, \cdots, C_{NN}^{(3)}\right)$. The variational formulation then becomes

$$\frac{1}{2}\begin{bmatrix}\mathbf{c}_1\\ \mathbf{c}_2\\ \mathbf{c}_3\end{bmatrix}^{\mathrm{t}} \mathbf{L} \begin{bmatrix}\mathbf{c}_1\\ \mathbf{c}_2\\ \mathbf{c}_3\end{bmatrix} = \mathbf{f}^{\mathbf{t}} \begin{bmatrix}\mathbf{c}_1\\ \mathbf{c}_2\\ \mathbf{c}_3\end{bmatrix} \tag{13}$$

where $\mathbf{L}$ is the matrix from the integrals and $\mathbf{f}$ is the vector of the external forcing, whose elements are given by

$$\int_0^A \int_0^B f(x,y)\phi_m(x)\psi_n(y)\,dx \tag{14}$$

with zero padding for the parts corresponding to $\mathbf{c}_2$ and $\mathbf{c}_3$. Here the forcing on the top plate is given by the Delta-function $f(x,y) = f_0\delta(x-x_0, y-y_0)$ for some fixed point (x_0, y_0) and a constant force amplitude f_0, which makes the integrals unnecessary. The following will give details how the elements of $\mathbf{L}$ are obtained.

Substituting the Fourier series expansion for the deflections w_1 and w_2 into Eq. (8) gives

$$\mathscr{P}_{1,2}^{\mathrm{slip}} = \sum_{j=1}^{S} \int_0^A \sigma_{\mathrm{slip}}(x,j) \left| h_1 \sum_{m,n=1}^{N} k_m C_{mn}^{(1)} \varphi_m(x)\psi_n(y_j) + h_2 \sum_{m=1}^{N} k_m C_{mj}^{(2)} \varphi_m(x) \right|^2 dx \tag{15}$$

where $\varphi_m(x) = \sqrt{2/A}\cos k_m x$. Then the above integral will be obtained by

$$\begin{aligned}&\int_0^A \sigma_{\mathrm{slip}}(x,j)\varphi_m(x)\varphi_{m'}(x)\,dx\\ &= \frac{1}{A}\int_0^A \sigma_{\mathrm{slip}}(x,j)\left(\cos\frac{\pi(m-m')}{A}x - \cos\frac{\pi(m+m')}{A}x\right)dx\end{aligned} \tag{16}$$

Notice that this integral is simply the Fourier cosine coefficients of the function $\sigma_{\mathrm{slip}}(x,j)$, which can be computed using the fast Fourier transform (FFT). The matrix that corresponds to the separation σ_{sep} can be obtained by the similar derivation. More details for calculating the elements of the matrix are given in Appendix .

Substituting the series expansion for $w_1(x,y)$ into Eq. (2) for $\mathscr{P}_1$ leads to vector and matrix expression for the strain energy of the top plate. Let the function D_1 be separated into $D_1(x,y) = \overline{D}_1 + d_1(x,y)$ where $\overline{D}_1$ is the average stiffness and $d_1(x,y)$ is the deviation from the average. The elements of the matrix $\mathbf{L}$ due to the varying stiffness $d_1(x,y)$ are computed using the integral

$$\sum_{\substack{m,n,\\ m',n'=1}}^{N} \int_0^A \int_0^B d_1(x,y) C_{mn}^{(1)} C_{m'n'}^{(1)} \left(k_m^2+\kappa_n^2\right)\left(k_{m'}^2+\kappa_{n'}^2\right) \times \phi_m(x)\phi_{m'}(x)\psi_n(y)\psi_{n'}(y)\,dxdy \tag{17}$$

The constant stiffness $\overline{D}_1$ will give us a diagonal matrix with its element $\overline{D}_1(k_m^2+\kappa_n^2)^2$ because of the orthogonality of the functions $\{\phi_m\}$ and $\{\psi_n\}$. The above integral is the formula for the Fourier cosine coefficients for the function $d_1(x,y)$, which can be found using the FFT. Furthermore, the products of *cosine* components are obtained by taking the real part of the FFT in x and y directions. The contribution from the bottom plate can be derived using the same formula for w_3.

In order to include not-so-straight shape of beams, we here make a few assumptions and keep the model simple. The strain energy of the beams is computed in the same way as before by integrating over the x from 0 to A. The shape of jth beam is denoted by the function of x, $\theta_j(x)$. Thus the contact between the top plate and the beam is given by $y = y_j + \theta_j(x)$. We first take the Taylor expansion of the basis functions along the junction and omit the higher order terms because $\theta_j(x)$ is assumed small.

$$\psi_n(y_j + \theta_j(x)) \approx \psi_n(y_j) + \kappa_n\theta_j(x)\chi_n(y_j) \tag{18}$$

where $\chi_n(y) = \sqrt{2/B}\cos\kappa_n y$. Then the displacement of the plate along the junction, denoted by B_j are given by

$$w_1|_{(x,y)\in B_j} = \sum_{m,n=1}^{N} \left\{\psi_n(y_j) + \kappa_n\theta_j(x)\chi_n(y_j)\right\} C_{mn}^{(1)}\phi_m(x) \tag{19}$$

The expansion for the twisting beams remains the same, i.e., $w_2(x,j) = \sum_{m=1}^{N} C_{mj}^{(2)}\phi_m(x)$. The energy contributions $\left\{\mathscr{P}_{i,j}^{\mathrm{slip}}, \mathscr{P}_{i,j}^{\mathrm{sep}}\right\}_{(i,j)=(1,2),(3,2)}$ are now calculated from the above two expressions.

The potential energy due to the slippage at the twisting beams is modified and given by

$$\mathscr{P}_{1,2}^{\mathrm{slip}} = \frac{\sigma_{\mathrm{slip}}}{2}\sum_{j=1}^{S}\int_0^A \frac{\left|h_1 w_1'(x, y_j+\theta_j(x)) + h_2 w_2'(x,j)\right|^2}{1+(\theta_j'(x))^2}\,dx \tag{20}$$

and the potential energy due to the separation is

$$\mathscr{P}_{1,2}^{\mathrm{sep}} = \frac{\sigma_{\mathrm{sep}}}{2}\int_0^A \left|w_1(x, y_j+\theta_j(x)) - w_2(x,j)\right|^2 dx \tag{21}$$

The constant σ_{sep} will be set to be large so to keep the plates and the beams in contact always. Here we assume that $|\theta_j(x)|^2 \ll 1$ and $|\theta_j'(x)|^2 \ll 1$. We then have the following simplified formula.

$$\mathscr{P}_{1,2}^{\mathrm{slip}} = \frac{\sigma_{\mathrm{slip}}}{2}\sum_{j=1}^{S}\int_0^A (h_1+h_2)^2\left|w_2'(x,j)\right|^2 dx \tag{22}$$

Substituting the series expansion of $w_2(x,j)$ gives

$$\mathscr{P}_{1,2}^{\text{slip}} = \frac{(h_1+h_2)^2}{2} \sum_{j=1}^{S} \sum_{m,m'=1}^{N} k_{mm'} C_{mj}^{(2)} C_{m'j}^{(2)} \times \int_0^A \sigma_{\text{slip}}(x,j) \varphi_m(x) \varphi_{m'}(x)\, dx \tag{23}$$

SIMULATION OF RANDOM FUNCTIONS

The parameter functions, $d_i(x,y)$, $\sigma_{\text{slip}}(x,j)$ and $\theta_j(x)$, must be continuous and smooth because they model real components and junctions. Thus a series of discrete random numbers along the junctions or a plate surface will not be adequate. The methods of generating continuous smooth random functions have been studied by the signal processing community for many years (see [5, 11, 12]). Here the random functions are simulated using the method given in [6], in which a stationary random process is simulated using a prescribed PDF and PSD. As an example, the Gaussian distribution is used for the prescribed PDF here. There are two reasons for the choice of Gaussian distribution. First, the computation of normally distributed random functions is simple. Second, the author has not been able to find any measurements of the PDF of stiffness of timber products and their junctions. However there is a set of data of timber beam shape (2.5 m long beams) obtained by SCION Research in New Zealand (through personal communication). The histogram of the twist amplitude is shown in Fig. 4. The standard deviation of the measurements is approximately 0.8 mm. 301 beams were measured at 500 positions. Figure 4 shows the histogram of the measurements at all positions.

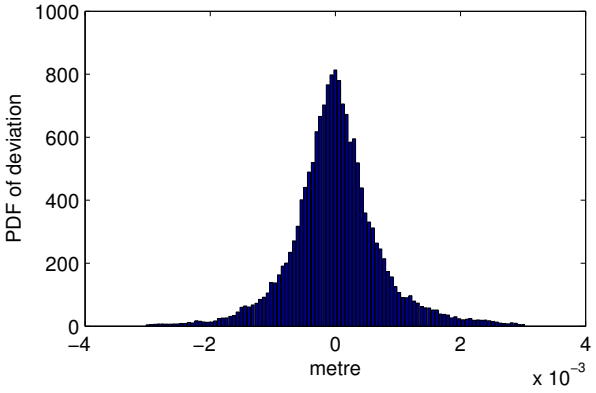

Figure 4. PDF of the twist of dried timber beams

Let $S(x)$ be a random function (or random process) for the spatial variable $0 \le x \le A$. We assume that $S(x)$ has the probability $p(S \le s)$ and the probability density function $p_S(s)$ at any $x \in [0,A]$. The PDF $p_S(s)$ is assumed to be identical for any x. In other words $S(x)$ is a stationary process. It is further assumed that $S(x)$ can be expressed by

$$S(x) = \sqrt{\frac{2}{M}} \sum_{i=1}^{M} Q_i \cos\left(2\pi F_i x/A + \Phi_i\right) \tag{24}$$

where Q_i, F_i, and Φ_i are the random variables with some probability densities. Here M needs to be sufficiently large, and is set to 100. The above series makes the mean of $S(x)$ zero for all $x \in [0,A]$. Let us follow the procedure given in [6] to formulate the PDFs for Q_i, F_i, and Φ_i.

First, the amplitudes $\{Q_i\}$ are assumed to be independent and identically distributed (i.i.d) random variable with PDF denoted by $p_Q(q)$ for $q > 0$. The phases $\{\Phi_i\}$ are also assumed to be i.i.d and their PDF is given by the uniform distribution in $[-\pi, \pi]$. The frequencies $\{F_i\}$ are i.i.d with the marginal first order continuous PDF denoted by $p_F(f)$ for $0 \le f \le V/2$.

The PDF of F_i and the PSD of $S(x)$ denoted by $P_S(f)$ are related by the formula

$$p_F(|f|) = \frac{2}{\mathbb{E}[Q^2]} P_S(f), \quad -\frac{V}{2} \le f \le \frac{V}{2} \tag{25}$$

where V is some large enough value so that $P_S(f)$ is nearly zero outside of the range $[-V/2, V/2]$. Setting the variance of S to be ν^2 gives $\mathbb{E}\left[Q^2\right] = \nu^2$. The PSD function $P_S(f)$ here is chosen to be simple bell shaped, for example, $P_S(f) = K \exp\left(-(f-\delta)^2/2\mu^2\right)$, where K, δ, and μ will be varied to simulate effects of changing parameters. An example is shown in Fig. 7(left).

The characteristic function of the random function $S(x)$ is given by

$$\psi_S(\gamma) = \mathbb{E}\left[e^{\mathrm{i}\gamma S}\right] = \left[\int_0^\infty p_Q(q) J_0\left(\frac{\gamma q}{\sqrt{M/2}}\right) dq\right]^M \tag{26}$$

where J_0 is the Bessel function of the first kind of order zero. The PDF for Q is related to the characteristic function of $S(x)$ by

$$p_Q(q) = q \int_0^\infty \left(\psi_S(v\sqrt{M/2})\right)^{1/M} J_0(qv) v\, dv \tag{27}$$

which is the inverse Hankel transform. For the Gaussian parameter, the characteristic function is given by $\psi_S(\gamma) = \exp\left(-\nu^2\gamma^2/2\right)$. Hence the inverse Hankel transform gives the following PDF of the amplitude

$$p_Q(q) = q \int_0^\infty \left(\exp\left(-\frac{M\nu^2}{4} v^2\right)\right)^{1/M} J_0(qv) v\, dv \tag{28}$$

The above integral has the closed form, which is

$$p_Q(q) = \frac{2q}{\nu^2} \exp\left(-\frac{q^2}{\nu^2}\right) \tag{29}$$

This is a Rayleigh PDF, which can be simulated from the two Gaussian random variables. For example, when the variance is $\nu^2 = 2$, then the amplitudes are simulated by $U_1 \sim \mathcal{N}(0,1)$ and $U_2 \sim \mathcal{N}(0,1)$, then $Q \sim \sqrt{U_1^2 + U_2^2}$. The histogram of the simulation result is shown in Fig. 5 along with the target PDF of normal distribution with the standard deviation $\sqrt{2}$. The slippage function $\sigma_{\text{slip}}(x,j)$ will be generated using the distribution shown in Fig. 5. The standard deviation of the distribution will be set to be 3×10^6 Nm^{-1}, which is 10% of the average slippage resistance constant 3×10^7 Nm^{-1}. This

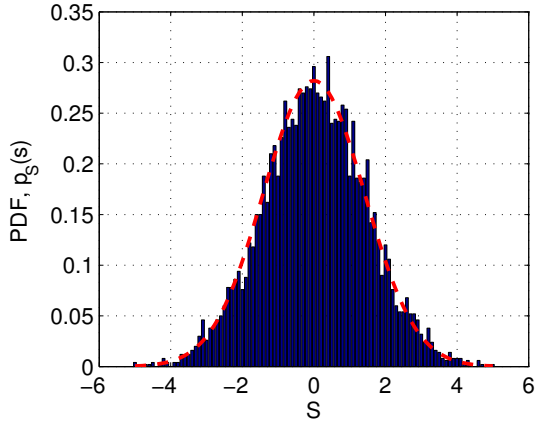

Figure 5. PDF of the simulated 1 dimensional function (not scaled) and target normal distribution (dashed) with standard deviation $\sqrt{2}$

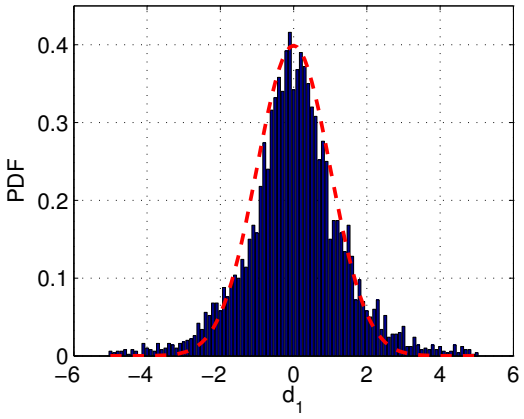

Figure 6. PDF (not scaled) of the simulated $d_1(1.2,1.2)$ and target normal distribution (dashed) with standard deviation 1

average value comes from the experimental measurements in [2] for the junction between a plywood panel and a timber joist.

The stiffness function $d_1(x,y)$ can be similarly simulated using the expansion

$$d_1(x,y) = \frac{1}{M}\sum_{i,j=1}^{M} Q_{ij}\cos\left(\frac{2\pi F_i x}{A}+\Phi_i\right)\cos\left(\frac{2\pi G_j y}{B}+\Psi_j\right) \tag{30}$$

where the coefficients $\{Q_{ij}\}$ are random variables with the Rayleigh distribution, and Φ_i and Ψ_j are uniformly distributed random values in $[-\pi,\pi]$. The frequencies F_i and G_j are also generated from Eq. (25) and Eq. (26). In order to prove that the above expression correctly simulates the random realization in 2-dimensional space with the correct PSD and PDF, one needs to extend the derivation given in [6], which is beyond the scope of this paper. Instead, only the simulated realizations are numerically confirmed here. The histogram of the simulations is shown in Fig. 6 with the target PDF of normal distribution with the standard deviation 1. Again the PSD of d_1 (and d_3) is chosen to be a simple bell shaped function. An example is shown in Fig. 7(right). In the numerical simulations, the standard deviation of the stiffness of the plates $d_1(x,y)$ and $d_3(x,y)$ will be set to be 3% of the average stiffness of the plates in the following section. The value 3% has been chosen because the effects of inhomogeneous stiffness start to show at that value.

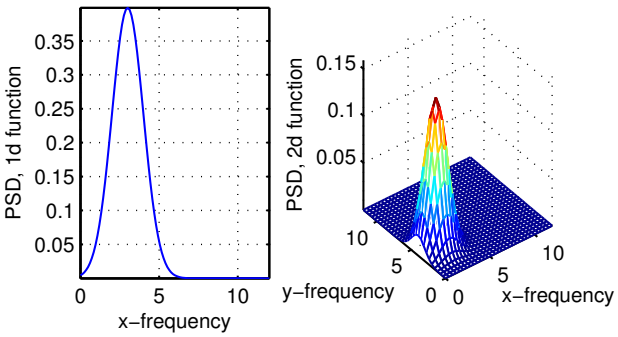

Figure 7. Examples of PSDs for the 1 and 2 dimensional random functions

NUMERICAL COMPUTATION

The computation results of the solution $w_1(x,y)$ are studied here using the simulated functions $\sigma_{\text{slip}}(x,j)$, $d_i(x,y)$ and $\theta_j(x)$. The number of terms for the Fourier expansion was set to be $N = 20$. All computation was done using MatLab on a standard personal desktop computer. No special numerical packages were used. The parameters for the beams and the plates are chosen from the well used values for plywood and timber beams, $E_1 = E_3 = 10^{10}$ Pa, $E_2 = 1.4\times10^{10}$ Pa, $m_1 = m_2 = m_3 = 500$ kgm^{-3}, $A = 5.1$ m, $B = 3.2$ m, $h_1 = h_3 = 0.015$ m, $h_2 = 0.3$ m, $\alpha = 0.3$, $y_j = jB/8$, $j = 1,2,...,7$, and the width of the beams is 0.045m. The average slippage constant is 3×10^7 Nm^{-1}, which was determined from the experiments in [2]. The location of the forcing is $(2.85,2.1)$ with $f_0 = 1000$N.

The PSD of random functions is chosen to mimic what might be happening at the junctions. It is not obvious to the author how the conditions can be measured in real composite structures. On the other hand, the PSD of the shape $\theta_j(x)$ may be chosen based on actual measurements. Here each PSD is simply set to be a bell shaped smooth curve with a peak (Fig. 7). Two different peak positions have been used to compare the effects of spatial variations on the solution.

Figures 8 and 9 show the distributions of the variance of the surface deflection of the top plate when slippage and stiffness are randomized, respectively. There seems to be no particular rule how the variance is distributed over the plate. The distribution varies as the frequency changes. The slippage affects lower frequency vibrations than it does the higher frequency ones as shown in Figs. 11(a) and (b). In Fig. 8, the variance distribution changes from even to localized distribution as the frequency increases. Figure 9 shows that the stiffness affects the higher frequency vibrations evenly over the plate. On the other hand the random stiffness shows localized effects at lower frequencies. Figure 10 shows the distributions of the variance of the surface deflection of the top plate when there is small random twist in the beams. The variance is more

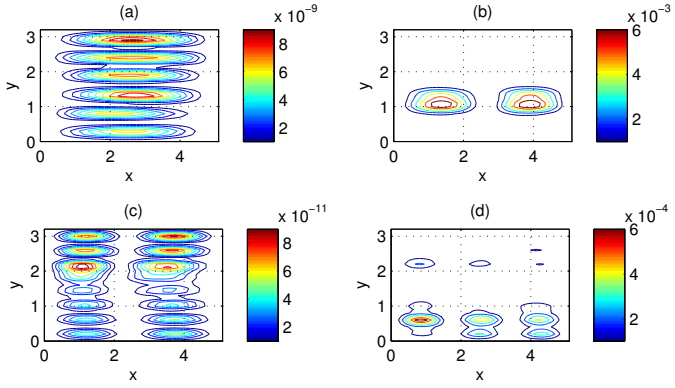

Figure 8. Contour plot of the variance distribution of the deflection over the top plate when slippage is random at 100 Hz (a), 150 Hz (b), 200 Hz (c) and 250 Hz (d)

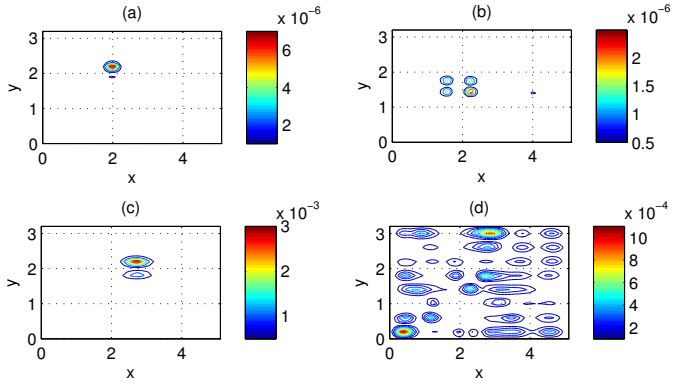

Figure 9. Contour plot of the variance distribution of the deflection over the top plate when stiffness of the two plates is random at 100 Hz (a), 150 Hz (b), 200 Hz (c) and 250 Hz (d)

evenly spread over the plate compared to Figs. 8 and 9.

Figures 11 and 12 show the root-mean-square velocity at the frequencies from 150 Hz to 250 Hz. The vertical axis is in a log scale without any reference velocity. The velocity is not converted to decibels because this study is not about sound pressure. The slippage is randomized for Figs. 11(a) and (b), and the stiffness is randomized for Figs. 11(c) and (d). Figures 11(a) and (b) correspond to the PSDs with peaks at spatial frequencies at 3 m^{-1} and 5 m^{-1}, respectively. Figures 11(c) and (d) correspond to the PSDs with peaks at spatial frequencies of (x,y) components at (2 m^{-1},4 m^{-1}) and (4 m^{-1},8 m^{-1}), respectively. The randomness of the slippage affects the surface velocity near the resonant frequencies at lower frequencies. However there is little effect showing between 220 Hz and 240 Hz, even thought there are several resonance frequencies in that range. The random stiffness affects the vibration at the higher frequencies and the vibration level is flattened. Furthermore the variance of the vibration level is small. In both slippage and stiffness cases, the smaller variations of the random functions lead to smoother vibration levels. Figure 12 shows the root-mean-square velocity when there is small random twist in the beams. The standard deviations of the twist are 1.25 mm (Fig. 12(a)) and 2.5 mm (Fig. 12(b)), which are

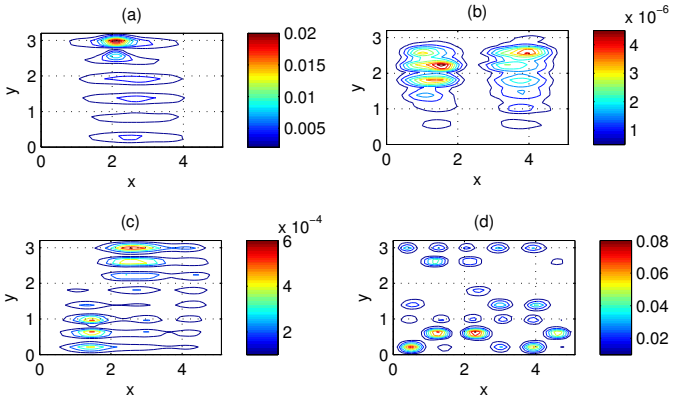

Figure 10. Contour plot of the variance distribution of the deflection over the top plate with the random twist in the beams at 100 Hz (a), 150 Hz (b), 200 Hz (c) and 250 Hz (d)

larger than the measured standard deviation shown in Fig. 4. The larger values were chosen to show clearly the effects of the twist. The larger twist affects the higher frequency vibrations in a similar way the random stiffness does in Fig. 11.

The numerical simulations show that the random irregularities affect the vibration over the whole plate surface. Thus the modelling of a composite structure, even this moderately complex double-leaf plate, requires the random irregularities to be taken into account. In particular, both Figs. 11 and 12 show that the vibrations at the higher frequencies are greatly affected by the random functions.

SUMMARY AND CONCLUSION

The simulations of the vibration of a double-leaf plate with random parameters have been carried out. The parameters are slippage, stiffness and small twist of beams, which are given by continuous smooth functions of x or (x,y). The computation cost of the simulations is kept low using the Fourier series solutions and the variational formulation. The simulations show that each random function affects the vibration differently in different ranges of frequencies. Also the spatial distributions of the variance show that the randomness along the junctions (slippage and twists) leads to more even spread over the plate than that of the random stiffness results. More definitive studies are needed to understand the effects of random parameters on the vibration. The method shown in this paper can include more random parameter functions as additional energy terms in the variational formulation. The method of solution changes little because only the elements of the matrix $\mathbf{L}$ in Eq. (13) that correspond to a new random function will need to be modified.

REFERENCES

[1] J. Brunskog, "The influence of finite cavities on the sound insulation of double-plate structures", *Journal of the Acoustical Society of America* **117**, 3727–3739 (2005)

[2] H. Chung and G. Emms, "Fourier series solutions to the vibration of rectangular lightweight floor/ceiling structures", *Acta Acustica United with Acustica* **94**, 401–409 (2008)

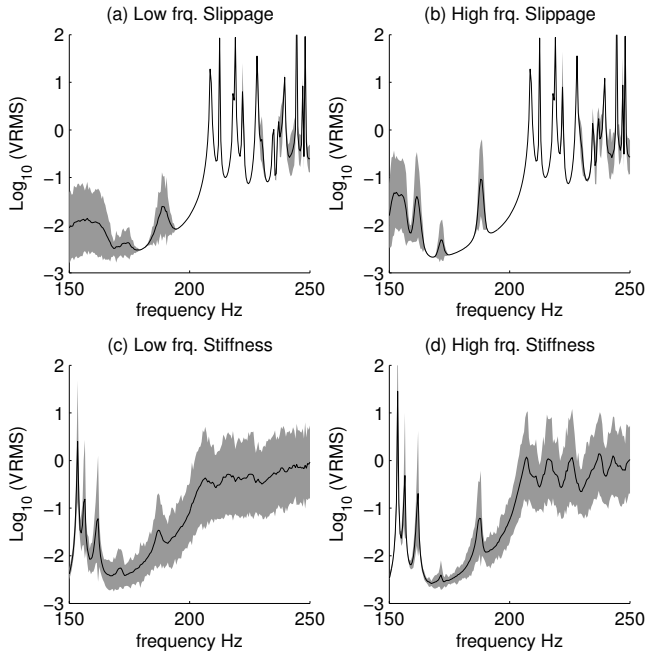

Figure 11. Velocity root mean square of when the slippage (a), (b) and the stiffness (c), (d) are randomized. The variance is shown by the gray area, and the mean of the simulations is shown by solid curve

[3] R.J.M. Craik, "Sound transmission through double leaf lightweight partitions. Part I: Airborne sound", *Applied Acoustics* **61**, 223–245 (2000)

[4] R.J.M. Craik, "Sound transmission through double leaf lightweight partitions. Part II: Structure-borne sound", *Applied Acoustics* **61**, 247–269 (2000)

[5] M. Grigoriu, "Simulation of stationary non-gaussian translation processes", *Journal of Engineering Mechanics* **124**, 121–126 (1998)

[6] S. Kay, "Representation and generation of non-gaussian wide-sense stationary random process with arbitrary PSDs and a class of PDFs", *IEEE Transactions on Signal Processing* **58**, 3448–3458 (2010)

[7] B.R. Mace, "Periodically stiffened fluid-loaded plates, I: Response to convected harmonic pressure and free wave propagation", *Journal of Sound and Vibration* **73**, 473–486 (1980)

[8] B.R. Mace, "Periodically stiffened fluid loaded plates, II: Response to line and point forces", *Journal of Sound and Vibration* **73**, 487–504 (1980)

[9] B.R. Mace, "Sound radiation from a plate reinforced by two sets of parallel stiffeners", *Journal of Sound and Vibration* **71**, 435–441 (1980)

[10] I.H. Shames and C.L. Dym, *Energy and finite element methods in structural mechanics*. Taylor & Francis, New York, SI units edition, 1991

[11] M. Shinozuka, "Simulation of multivariate and multidimensional random process", *Journal of the Acoustical Society of America*, **49**, 357–368 (1971)

[12] M. Shinozuka and C.M. Jan, "Digital simulation of random processes and its applications", *Journal of Sound and Vibration* **25**, 111–128 (1972)

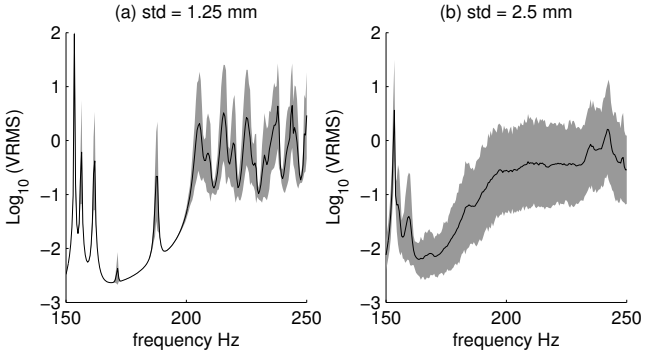

Figure 12. The root-mean-square velocity when there is small random twist in the beams. The variance is shown by the gray area, and the mean of the simulations is shown by solid curve

Appendix - Formulae for the simple coupling between a plate and beams

When the coupling parameter σ_{sep} is constant along the beams, the lagrangian matrix for the coupling energy contribution is given by

$$\frac{\sigma_{\text{sep}}}{2}\sum_{j=1}^{S}\int_0^A \left|w_1(x,y_j)-w_2(x,j)\right|^2 dx \tag{A1}$$

The above expression can be expressed by the vector operation

$$\frac{1}{2}\begin{pmatrix}\mathbf{c}_1\\ \mathbf{c}_2\end{pmatrix}^{\text{t}}\begin{bmatrix}\sigma_{\text{sep}}M^{\text{t}}M & -\sigma_{\text{sep}}M^{\text{t}}\\ -\sigma_{\text{sep}}M & \sigma_{\text{sep}}I\end{bmatrix}\begin{pmatrix}\mathbf{c}_1\\ \mathbf{c}_2\end{pmatrix} \tag{A2}$$

where the matrix M represents the operation

$$\sum_{n=0}^{N} C_{mn}^{(1)}\psi_n(y_j) \tag{A3}$$

Then, the total matrix is given by

$$\begin{bmatrix}L_1+\sigma_{\text{sep}}M^{\text{t}}M & -\sigma_{\text{sep}}M^{\text{t}}\\ -\sigma_{\text{sep}}M & L_2+\sigma_{\text{sep}}I\end{bmatrix} \tag{A4}$$

where I is the identity matrix. The matrices for the interaction between the beams and the bottom plate can be obtained in a similar way. We have the complete matrix

$$\begin{bmatrix}L_1+\sigma_{\text{sep}}M^{\text{t}}M & -\sigma_{\text{sep}}M^{\text{t}} & 0\\ -\sigma_{\text{sep}}M & L_2+2\sigma_{\text{sep}}I & -\sigma_{\text{sep}}M\\ 0 & -\sigma_{\text{sep}}M^{\text{t}} & L_3+\sigma_{\text{sep}}M^{\text{t}}M\end{bmatrix} \tag{A5}$$

where L_i, $i=1,2,3$ are the strain and kinetic energy matrices for the top plate, the beams, and the bottom plate, respectively.